J. Fluid Mech. (1998), *vol.* 358, *pp.* 357–378. Printed in the United Kingdom

© 1998 Cambridge University Press

Tertiary solutions and their stability in rotating plane Couette flow

By M. NAGATA

School of Mathematics and Statistics, The University of Birmingham, Edgbaston, Birmingham, B15 2TT, UK

(Received 27 January 1997 and in revised form 21 November 1997)

The stability of nonlinear tertiary solutions in rotating plane Couette flow is examined numerically. It is found that the tertiary flows, which bifurcate from two-dimensional streamwise vortex flows, are stable within a certain range of the rotation rate when the Reynolds number is relatively small. The stability boundary is determined by perturbations which are subharmonic in the streamwise direction. As the Reynolds number is increased, the rotation range for the stable tertiary motions is destroyed gradually by oscillatory instabilities. We expect that the tertiary flow is overtaken by time-dependent motions for large Reynolds numbers. The results are compared with the recent experimental observation by Tillmark & Alfredsson (1996).

1 Introduction

Shear motions of fluids are affected by system rotation. Understanding the effect of the Coriolis force on transition from laminar shear motions to turbulence is of considerable importance in designing rotating devices in engineering and industrial applications (Bradshaw 1969, 1988), and in resolving mechanisms of natural phenomena in geophysical and astrophysical studies (Tritton 1978, 1985; Tritton & Davies 1981; Hopfinger 1989; Hopfinger & Linden 1990).

It is well known that for rotating channel flows with the rotation vector in the spanwise direction, the Squire theorem does not hold and streamwise-independent disturbances are responsible for the onset of secondary motions in general (see Hart 1971 and Lezius & Johnston 1976; for example). The secondary motions take the form of roll cells (streamwise vortex flows), which are streamwise independent and regularly spaced in the spanwise direction. Subsequent development of the flows is characterized by three-dimensional motions with dominant streamwise vortex structures (see Alfredsson & Persson 1989; Finlay 1989, 1990; Yang & Kim 1991; for rotating Poiseuille flow).

Recently, preliminary experimental investigations have been carried out on rotating plane Couette flow by Tillmark & Alfredsson (1996). They report that for a fixed rotation rate the roll cells with spanwise width approximately equal to the gap between the two plates break down to a wavy vortex structure with the streamwise wavelength approximately three times the spanwise width of the vortex as the strength of the shear is increased.

Mathematically, the problem of plane Couette flow under system rotation is identical to that of the narrow gap limit of the almost co-rotating Taylor–Couette system. The bifurcation sequence and the transition of the latter have been investigated intensively by Nagata (1986, 1988). By 'almost co-rotating' it is meant that the two

concentric cylinders rotate with almost equal angular velocities. We briefly summarize Nagata's findings below. With the background rotation Ω, the stability of the basic flow is determined by a single non-dimensional parameter, called the Taylor number,

$$T = \Omega(R - \Omega), \tag{1.1}$$

where R, to be defined in the next section, is the Reynolds number (a measure of the shear strength across the fluid layer). At the critical Taylor number, T_c, a secondary flow characterized by two-dimensional steady streamwise vortex motions bifurcates. The value of T_c is 1708 and the corresponding critical spanwise wavenumber β_c is 3.116. Provided that $T_c = \Omega(R - \Omega)$ yields two real roots $\Omega = \Omega_c^{(1)}$ and $\Omega = \Omega_c^{(2)}$ for a fixed R, secondary flow exists for $\Omega_c^{(1)} \leqslant \Omega \leqslant \Omega_c^{(2)}$. For $R^2 \gg 4T_c$ the two roots are approximately $\Omega_c^{(1)} \simeq 0$ and $\Omega_c^{(2)} \simeq R$. Since the almost co-rotation assumption is only applicable near the Rayleigh line, $R = \Omega$, instabilities of the two-dimensional steady streamwise vortex flow were examined near $\Omega = \Omega_c^{(2)}$. Four different types of three-dimensional flows are identified theoretically and their onset in the (Ω, R)-plane is in good agreement with the experimental observation by Andereck, Dickman & Swinney (1983). They are twisted vortices, wavy vortices, wavy-inflow-boundary flows and wavy-outflow-boundary flows. Further, recognizing that the limit $\Omega \to 0$ corresponds to non-rotating plane Couette flow exactly, Nagata (1990) extended his analysis to the region near $\Omega = \Omega_c^{(1)}$, although the assumption of almost co-rotation is violated for small Ω. He found a tertiary solution branch connecting two points $\Omega = \Omega_1$ and $\Omega = \Omega_2$, where the secondary flow loses its stability. (Thus, the secondary flow is stable in the two separate intervals $\Omega_c^{(1)} < \Omega < \Omega_1$ and $\Omega_2 < \Omega < \Omega_c^{(2)}$.) The tertiary solutions are steady and three-dimensional with a non-zero streamwise wavenumber α. They bifurcate at $\Omega = \Omega_1$ and $\Omega = \Omega_2$ supercritically for relatively small Reynolds numbers. For a larger Reynolds number the bifurcation at Ω_1 becomes subcritical. The subcritical nature of the tertiary solution branch led to the discovery of nonlinear plane Couette flow solutions at $\Omega = 0$.

It should be emphasized that the rectangular coordinate system used by Nagata is applicable to any part of the (Ω, R)-plane in the case of rotating plane Couette flow. We re-examine the nonlinear tertiary solutions in the system for small Ω and analyse their stability, which has not been done so far. We shall locate the stability region of the steady tertiary motions on the (α, Ω)-space for selected values of R. We attempt to compare results with available experimental observation.

2 Formulation of the problem

We consider a fluid motion between two parallel plates separated by the distance L. The bottom plate moves along in its own plane, indicated by the x-direction in figure 1, with a constant speed $\frac{1}{2}U_0$, whereas the top plate moves in the negative x-direction with the same speed. A constant spanwise rotation Ω_0 in the y-direction is imposed on the system. We assume that the fluid is viscous and incompressible with a constant density ρ and the kinematic viscosity ν.

The fluid motion is governed by the equation of continuity,

$$\nabla \cdot \boldsymbol{u} = 0, \tag{2.1}$$

and the conservation of momentum,

$$\frac{\partial \boldsymbol{u}}{\partial t} + \boldsymbol{u} \cdot \nabla \boldsymbol{u} + \Omega \boldsymbol{j} \times \boldsymbol{u} = -\nabla p + \nabla^2 \boldsymbol{u}, \tag{2.2}$$

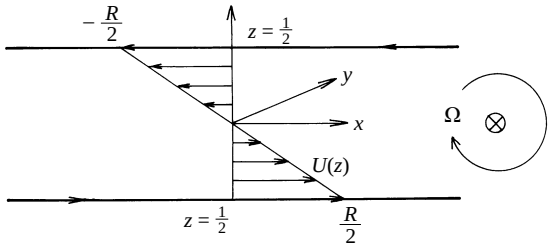

FIGURE 1. Non-dimensional physical configuration.

where the velocity $\boldsymbol{u}$ and the pressure p are normalized by v/L and $\rho v^2/L^2$. The time t and the position vector $\boldsymbol{r} = (x\boldsymbol{i} + y\boldsymbol{j} + z\boldsymbol{k})$ with $\boldsymbol{i}, \boldsymbol{j}, \boldsymbol{k}$ being the unit direction vectors have been non-dimensionalized by using the time scale for the viscous dissipation L^2/v and the length scale L. The no-slip condition is prescribed on the plates at $z = \pm\frac{1}{2}$:

$$\boldsymbol{u} = \mp\tfrac{1}{2}R\boldsymbol{i}. \tag{2.3}$$

Thus, the non-dimensional parameters controlling the system are the Reynolds number,

$$R = \frac{U_0 L}{v}, \tag{2.4}$$

and the rotation rate,

$$\Omega = \frac{2\Omega_0 L^2}{v}. \tag{2.5}$$

The unidirectional flow

$$\boldsymbol{u} = U(z)\boldsymbol{i}, \tag{2.6}$$

satisfies (2.1), (2.2) and (2.3) exactly with

$$U(z) = -Rz. \tag{2.7}$$

We are concerned with the situation where $\boldsymbol{u}$ deviates from this basic state.

After introducing a velocity fluctuation $\hat{\boldsymbol{u}}$, we operate with $\boldsymbol{k}\cdot\nabla\times\nabla\times$, and $\boldsymbol{k}\cdot\nabla\times$ on (2.2):

$$(U\partial_x - \nabla^2 + \partial_t)\nabla^2\Delta_2\phi - U''\partial_x\Delta_2\phi + \Omega\partial_y\Delta_2\psi + \boldsymbol{k}\cdot\nabla\times\nabla\times[\hat{\boldsymbol{u}}\cdot\nabla\hat{\boldsymbol{u}}] = 0, \tag{2.8}$$

$$(U\partial_x - \nabla^2 + \partial_t)\Delta_2\psi - U'\partial_y\Delta_2\phi - \Omega\partial_y\Delta_2\phi - \boldsymbol{k}\cdot\nabla\times[\hat{\boldsymbol{u}}\cdot\nabla\hat{\boldsymbol{u}}] = 0, \tag{2.9}$$

where $\Delta_2 = (\partial_x)^2 + (\partial_y)^2$ is the two-dimensional Laplacian operator, and ϕ and ψ represent the poloidal and the toroidal parts of the solenoidal fluctuation $\hat{\boldsymbol{u}}$:

$$\hat{\boldsymbol{u}} = \nabla\times\nabla\times\boldsymbol{k}\phi + \nabla\times\boldsymbol{k}\psi. \tag{2.10}$$

The boundary conditions at $z = \pm\frac{1}{2}$ now become

$$\phi = \partial_z\phi = \psi = 0. \tag{2.11}$$

3 Nonlinear steady tertiary solution

In this section we briefly repeat the analysis by Nagata (1990). In order to describe three-dimensional nonlinear steady states we separate $\hat{\boldsymbol{u}}$ into the average part $\breve{U}(z)$

$$\breve{U}(z)\boldsymbol{i} = \bar{\hat{\boldsymbol{u}}}, \tag{3.1}$$

where the overbar denotes the xy-average, and the residual

$$\check{\boldsymbol{u}} = \hat{\boldsymbol{u}} - \check{U}(z)\boldsymbol{i} = \nabla \times \nabla \times \boldsymbol{k}\phi + \nabla \times \boldsymbol{k}\psi. \tag{3.2}$$

There should be no confusion in using the same notations, ϕ and ψ, as in (2.10) with different definitions. Owing to (3.1) we impose

$$\overline{\phi} = \overline{\psi} = 0. \tag{3.3}$$

We expand ϕ, ψ and $\check{U}$ in each of the three spatial directions in terms of an appropriate set of orthogonal functions, i.e.

$$\phi = \sum_{\ell=1}^{\infty} \sum_{m=-\infty}^{\infty} \sum_{n=-\infty}^{\infty} a_{\ell m n} \mathrm{e}^{\mathrm{i}m\alpha x} \mathrm{e}^{\mathrm{i}n\beta y} f_\ell(z), \tag{3.4}$$

$$\psi = \sum_{\ell=1}^{\infty} \sum_{m=-\infty}^{\infty} \sum_{n=-\infty}^{\infty} b_{\ell m n} \mathrm{e}^{\mathrm{i}m\alpha x} \mathrm{e}^{\mathrm{i}n\beta y} \sin \ell\pi(z + \tfrac{1}{2}), \tag{3.5}$$

$$\check{U} = \sum_{k=1}^{\infty} c_k \sin 2k\pi(z + \tfrac{1}{2}). \tag{3.6}$$

Because of (3.3), the components of ϕ, ψ with $m = n = 0$ must be incorporated in $\check{U}$, and hence they are disregarded from the summations in (3.4) and (3.5). In the expression (3.4), $f_\ell(z)$, which was introduced by Chandrasekhar (1961), is symmetric/antisymmetric in z for ℓ equal to an odd/even integer. It satisfies $f_\ell(\pm\frac{1}{2}) = f'_\ell(\pm\frac{1}{2}) = 0$ (see (23a) of Nagata 1986). Note that $\sin \ell\pi(z + \frac{1}{2})$ in (3.5) is also symmetric/antisymmetric in z depending on ℓ being odd/even. Owing to the symmetry of the system, $\check{U}$ is antisymmetric in z for any k.

The steadiness in (2.8) and (2.9) requires

$$(\hat{U}\partial_x - \nabla^2)\nabla^2\Delta_2\phi - \hat{U}''\partial_x\Delta_2\phi + \Omega\partial_y\Delta_2\psi + \boldsymbol{k} \cdot \nabla \times \nabla \times [\check{\boldsymbol{u}} \cdot \nabla\check{\boldsymbol{u}}] = 0, \tag{3.7}$$

$$(\hat{U}\partial_x - \nabla^2)\Delta_2\psi - \hat{U}'\partial_y\Delta_2\phi - \Omega\partial_y\Delta_2\phi - \boldsymbol{k} \cdot \nabla \times [\check{\boldsymbol{u}} \cdot \nabla\check{\boldsymbol{u}}] = 0, \tag{3.8}$$

where

$$\hat{U}(z) = U(z) + \check{U}(z) \tag{3.9}$$

is the mean velocity field distorted by the nonlinear interactions between the components of ϕ and ψ.

After substituting (3.4), (3.5) and (3.6) in (3.7) and (3.8), we multiply them by $\exp(-\mathrm{i}\mu\alpha x)\exp(-\mathrm{i}\nu\beta y)f_\lambda(z)$ and $\exp(-\mathrm{i}\mu\alpha x)\exp(-\mathrm{i}\nu\beta y)\sin\lambda\pi(z+\frac{1}{2})$, respectively, and average the results over the fluid layer. The integers μ, ν and λ run through all the admissible values. Since the case where both μ and ν are zero at the same time is not admissible in (3.7) and (3.8), we must derive an additional equation for $\check{U}$. This is accomplished by the xy-average of the x-component of (2.2),

$$(d_z)^2\check{U} + d_z\overline{\Delta_2\phi(\partial^2_{xz}\phi + \partial_y\psi)} = 0, \tag{3.10}$$

where (2.1) is used in the derivation. We multiply (3.10) by $\sin 2\kappa\pi(z + \frac{1}{2})$ for all the admissible integers κ and integrate the result over the entire depth of the fluid layer. The integrals involved in this Galerkin procedure are evaluated analytically.

We note that the boundary conditions

$$\phi = \partial_z \phi = \psi = \check{U} = 0 \tag{3.11}$$

at $z = \pm\frac{1}{2}$ are satisfied by (3.4), (3.5) and (3.6).

The nonlinear differential equations (3.7), (3.8) and (3.10) have now been transformed into an infinite set of nonlinear algebraic equations for $a_{\ell mn}$, $b_{\ell mn}$ and c_k. The reality condition requires

$$a^*_{\ell\,-m\,-n} = a_{\ell\,m\,n}, \qquad b^*_{\ell\,-m\,-n} = b_{\ell\,m\,n}, \tag{3.12}$$

where the asterisk * denotes the complex conjugate. The system is further simplified by its symmetry: it can be found that the set $\mathscr{A}_2$ in the Appendix (A 1) is closed for the nonlinear interactions among its components (see Nagata 1986).

For numerical purposes the infinite series in (3.4), (3.5) and (3.6) must be truncated so that only those components with $a_{\ell mn}$, $b_{\ell mn}$ and c_k are taken into account, if their subscripts satisfy

$$\ell + |m| + |n| < N_T, \qquad k < N'_T. \tag{3.13}$$

The resulting finite set of nonlinear algebraic equations

$$A_{ij} x_j + B_{ijk} x_j x_k = 0, \tag{3.14}$$

is solved using the Newton–Raphson iteration method, where the matrix A_{ij} and the third-order tensor B_{ijk} are functions of α, β, R, and Ω, and x_j represents a vector whose elements are the amplitudes $a_{\ell mn}$, $b_{\ell mn}$ and c_k.

The numerical convergence of the three-dimensional nonlinear solution at $\Omega = 20$ and $R = 200$ is examined with respect to three truncation levels in table 1, where the momentum transport

$$M_t = -d_z \hat{U} \tag{3.15}$$

on the boundary $z = \pm\frac{1}{2}$ is used as a nonlinear measure of the solution. For larger R higher truncation levels are required to obtain higher accuracy. The truncation formula (3.13) has the advantage of reducing the dimension of the system as much as possible without missing out vital information for the study of bifurcation (Nagata 1986, 1988, 1990).

4 Stability of the steady tertiary solution

In order to analyse the stability of the steady tertiary solutions in §3, we superimpose perturbations

$$\tilde{\boldsymbol{u}} = \nabla \times \nabla \times \boldsymbol{k}\tilde{\phi} + \nabla \times \boldsymbol{k}\tilde{\psi} \tag{4.1}$$

of infinitesimal magnitude on $\hat{\boldsymbol{u}}$, substitute $\boldsymbol{u} = \hat{\boldsymbol{u}} + \tilde{\boldsymbol{u}}$ into (2.8) and (2.9), and linearize the resulting equations with respect to $\tilde{\boldsymbol{u}}$:

$$(\hat{U}\partial_x - \nabla^2 + \partial_t)\nabla^2\Delta_2\tilde{\phi} - \hat{U}''\partial_x\Delta_2\tilde{\phi} + \Omega\partial_y\Delta_2\tilde{\psi} + \boldsymbol{k}\cdot\nabla\times\nabla\times[\tilde{\boldsymbol{u}}\cdot\nabla\check{\boldsymbol{u}} + \check{\boldsymbol{u}}\cdot\nabla\tilde{\boldsymbol{u}}] = 0, \tag{4.2}$$

$$(\hat{U}\partial_x - \nabla^2 + \partial_t)\Delta_2\tilde{\psi} - \hat{U}'\partial_y\Delta_2\tilde{\phi} - \Omega\partial_y\Delta_2\tilde{\phi} - \boldsymbol{k}\cdot\nabla\times[\tilde{\boldsymbol{u}}\cdot\nabla\check{\boldsymbol{u}} + \check{\boldsymbol{u}}\cdot\nabla\tilde{\boldsymbol{u}}] = 0. \tag{4.3}$$

Since $\check{\boldsymbol{u}}$ is periodic in the x- and y-directions, perturbations $\tilde{\phi}$ and $\tilde{\psi}$ must have the following expressions (Floquet theory):

$$\tilde{\phi} = \sum_{\ell=1}^{\infty}\sum_{m=-\infty}^{\infty}\sum_{n=-\infty}^{\infty} \tilde{a}_{\ell\,m\,n} \mathrm{e}^{\mathrm{i}m\alpha x}\mathrm{e}^{\mathrm{i}n\beta y} f_\ell(z)\mathrm{e}^{\mathrm{i}dx+\mathrm{i}by}\mathrm{e}^{\sigma t}, \tag{4.4}$$

N_T, N'_T	M_t	dim $\boldsymbol{x}$
12,10	1.631 595 9	445
13,11	1.631 593 3	589
14,12	1.631 513 6	734

TABLE 1. The momentum transport M_t of the three-dimensional solution. $\alpha = 1.0$, $\beta = 3.117$, $R = 200$, $\Omega = 20$

$$\tilde{\psi} = \sum_{\ell=1}^{\infty} \sum_{m=-\infty}^{\infty} \sum_{n=-\infty}^{\infty} \tilde{b}_{\ell mn} \mathrm{e}^{\mathrm{i}m\alpha x} \mathrm{e}^{\mathrm{i}n\beta y} \sin \ell\pi(z + \tfrac{1}{2}) \mathrm{e}^{\mathrm{i}dx + \mathrm{i}by} \mathrm{e}^{\sigma t}, \tag{4.5}$$

where α and β are equal to the wavenumbers of the steady tertiary solution. The boundary conditions

$$\tilde{\phi} = \partial_z \tilde{\phi} = \tilde{\psi} = 0 \tag{4.6}$$

at $z = \pm\frac{1}{2}$ are satisfied by (4.4) and (4.5). In contrast to the ϕ and ψ of the steady solutions, $\tilde{a}_{\ell 00}$ and $\tilde{b}_{\ell 00}$ are permissible in (4.2) and (4.3), provided $d \neq 0$ and $b \neq 0$. Equations (4.2) and (4.3) constitute the eigenvalue problem with the growth rate σ as the eigenvalue for a given Floquet parameter pair d and b.

When the symmetry of the steady solution is described by $\mathscr{A}_2$, perturbation equations (4.2) and (4.3) allow us to separate the linearly interacting components of $\tilde{\phi}$ and $\tilde{\psi}$ into the classes A and B for $d = 0$ and $b \neq 0$, and the classes C and D for $d \neq 0$ and $b = 0$ (see the Appendix). When $db \neq 0$, classes A and B unite and so do classes C and D. The resulting two united sets are identical.

In order to establish the eigenvalue problem in terms of $\tilde{a}_{\ell mn}$ and $\tilde{b}_{\ell mn}$, we multiply (4.2) and (4.3) by the same functions as we used in the process of deriving nonlinear algebraic equations for the steady flows, and average the result over the fluid layer.

The NAG routine F02BJF is used to solve the resulting eigenvalue problem

$$P_{ij}\tilde{x}_j = \sigma Q_{ij}\tilde{x}_j, \tag{4.7}$$

where $\tilde{x}_j$ represents a vector whose elements are $\tilde{a}_{\ell mn}$, and $\tilde{b}_{\ell mn}$. The matrices P_{ij} and Q_{ij} are functions of the Floquet parameters d and b and the nonlinear solution $a_{\ell mn}$, $b_{\ell mn}$ and c_k with the wavenumbers α and β at R and Ω.

For consistency the truncation level of (4.7) should be the same as that of (3.14) for fixed α, β, R, and Ω. The dimension of $\tilde{\boldsymbol{x}}$ is almost twice as large as that of $\boldsymbol{x}$ in the case of either $d = 0$ or $b = 0$, and four times larger in the case of $db \neq 0$ (see, for example, the level $N_T = 12$ in tables 1 and 2). Unless specified, the truncation numbers $N_T = 14$ and $N'_T = 12$ for $db = 0$, and $N_T = 12$ and $N'_T = 10$ for $db \neq 0$, are chosen. In the case of $db \neq 0$, the FORTRAN programme to solve (4.7) with vectorization and optimization requires 150 minutes cpu time on the IBM3090 at the University of Birmingham for $N_T = 12$, and 3 hours cpu time on the Convex C3840 at University of London Computer Centre for $N_T = 13$.

The numerical convergence of the growth rate σ with the largest real part is checked in table 2 for various combinations of the Floquet parameter pair d and b of the perturbations at $\Omega = 20$ and $R = 200$.

Let $\sigma_i(d, b)$, (i = A, B, C and D) denote the eigenvalue as a function of the Floquet parameters d and b for the classes A, B, C and D when α, β, R and Ω are fixed. By (4.4) and (4.5) $\sigma_i(0, -b) = \sigma_i(0, b)$ for i = A and B, and $\sigma_i(-d, 0) = \sigma_i(d, 0)$ for i = C and D. From (A 4) and (A 5) $\sigma_B(0, b \pm \beta) = \sigma_A(0, b)$ because $n''\beta \pm \beta$

N_T	σ	dim $\tilde{\boldsymbol{x}}$
(a) : $(d,b) = (0, 0.779)$, Class A		
12	$(-9.7581, 0)$	902
13	$(-9.7597, 0)$	1144
14	$(-9.7589, 0)$	1482
(b) : $(d,b) = (0, 0.779)$, Class B		
12	$(-1.3244, 0)$	880
13	$(-1.3245, 0)$	1168
14	$(-1.3245, 0)$	1456
(c) : $(d,b) = (0.5, 0)$, Class C		
12	$(-0.10252, 0)$	891
13	$(-0.09566, 0)$	1156
14	$(-0.09809, 0)$	1469
(d) : $(d,b) = (0.5, 0)$, Class D		
12	$(-0.10557, 0)$	891
13	$(-0.09525, 0)$	1156
14	$(-0.09873, 0)$	1469
(e) : $(d,b) = (0.5, 0.779)$		
10	$(-9.536\,726, \pm 17.239\,61)$	978
11	$(-9.417\,305, \pm 17.304\,09)$	1340
12	$(-9.448\,437, \pm 17.297\,80)$	1782
13	$(-9.438\,069, \pm 17.302\,32)$	2312

TABLE 2. The growth rate σ; $\alpha = 1.0$, $\beta = 3.117$, $R = 200$, $\Omega = 20$. The first/second entry in the bracket represents the real/imaginary part of σ

	$d = 0,\ b = 0.779$	$d = 0,\ b = 0.779 + \beta$
σ_A	$(-9.758, 0)$	$(-1.318, 0)$
σ_B	$(-1.324, 0)$	$(-9.753, 0)$
	$d = 0.5,\ b = 0$	$d = 0.5 + \alpha,\ b = 0$
σ_C	$(-0.098\,09, 0)$	$(-0.096\,53, 0)$
σ_D	$(-0.098\,73, 0)$	$(-0.096\,44, 0)$
	$d = 0.251,\ b = 0.779$	$d = 0.251,\ b = 0.779 + \beta$
σ	$(-8.583, \pm 3.908)$	$(-8.572, \pm 3.902)$

TABLE 3. The periodicity of the growth rate σ; $\alpha = 1.0$, $\beta = 3.117$, $R = 200$, $\Omega = 20$. $N_T = 12$. The first/second entry in the bracket represents the real/imaginary part of σ

becomes $n'\beta$ and $n'\beta \pm \beta$ becomes $n''\beta$. Similarly, $\sigma_D(d \pm \alpha, 0) = \sigma_C(d, 0)$. In particular, if $d = -\frac{1}{2}\alpha$, then $\sigma_D(\frac{1}{2}\alpha, 0) = \sigma_C(-\frac{1}{2}\alpha, 0) = \sigma_C(\frac{1}{2}\alpha, 0)$. Similarly, if $d = \frac{1}{2}\alpha$, then $\sigma_D(\frac{3}{2}\alpha, 0) = \sigma_D(-\frac{1}{2}\alpha, 0) = \sigma_C(-\frac{3}{2}\alpha, 0) = \sigma_C(\frac{3}{2}\alpha, 0)$. These relations are confirmed in table 3.

Since $\sigma_A(0, \frac{1}{2}\beta + b) = \sigma_A(0, -\frac{1}{2}\beta - b) = \sigma_B(0, \frac{1}{2}\beta - b)$ and similarly $\sigma_C(\frac{1}{2}\alpha + d, 0) = \sigma_D(\frac{1}{2}\alpha - d, 0)$, it is sufficient to evaluate σ in the (d, b)-space only for $0 \leqslant d \leqslant \alpha/2$ and $0 \leqslant b \leqslant \beta/2$.

5 Results

We first obtain streamwise vortex flows, $\mathscr{U}_0$ in the Appendix (A 2), with $\alpha = 0$ and $\beta = 3.117$. They bifurcate supercritically from the laminar basic state at $\Omega = \Omega_c$. Then, the stability of the streamwise vortex flows to the general form of three-dimensional perturbations is analysed. (These perturbations correspond to classes C and D in the Appendix with the restriction to $m'' = 0$ only. They are classified as $\tilde{\mathscr{U}}_I$ and $\tilde{\mathscr{U}}_{II}$ in Nagata 1986.) We denote the eigenvalue for these three-dimensional perturbations $\tilde{\sigma}$. The values of d and b which are responsible for the instability predict the wavenumbers of bifurcating tertiary flows. Instabilities for small Ω occur at $d \neq 0$ and $b = 0$ in general with $\mathrm{Im}[\tilde{\sigma}] = 0$ in the class $\tilde{\mathscr{U}}_{II}$, so that the tertiary flows are expected to be steady and three-dimensional with the symmetry $\mathscr{A}_2$ (see Nagata 1986, 1988 for details). After obtaining the tertiary solutions (3.4)–(3.6), we analyse their stability by calculating the eigenvalue σ of three-dimensional perturbations (4.4) and (4.5).

5.1 $R = 200$

The streamwise vortex flow ($\alpha = 0, \beta = 3.117$) bifurcates supercritically at $\Omega_c^{(1)} = 8.94$ as the rotation parameter Ω is increased from zero for $R = 200$. The stability of the nonlinear streamwise vortex flows is examined for various values of the Floquet parameters d and b of the superimposed perturbations. It is found that the growth rate $\tilde{\sigma}$ becomes positive for $d \neq 0$ and $b = 0$ as Ω is increased from Ω_c. Figure 2 shows $\tilde{\sigma}$ as a function of Ω for four different values of d with $b = 0$. Perturbations with $d = 1.5, 2.0$ never grow, whereas those with $d = 1.0, 0.5$ have a positive growth rate in a finite interval $\Omega_1 < \Omega < \Omega_2$ above $\Omega_c^{(1)}$. (The values of Ω_1 and Ω_2 depend on d.) As d is decreased from, say 0.5, the lower limit, Ω_1, of the unstable interval $\Omega_1 < \Omega < \Omega_2$ becomes small monotonically. The minimum value of Ω_1, $\min[\Omega_1(d)] = 9.96$, is found to be determined as $d \to 0$ so that there exists a small interval of Ω immediately above Ω_c where $\tilde{\sigma} < 0$ for any $d \neq 0$. Note that the streamwise vortex flow always has zero eigenvalue for perturbations with the same spatial structure (i.e. $d = 0$ and $b = 0$) as itself: it is neutrally stable to translational deviations. As d deviates from zero, the growth rate becomes negative at $\Omega = \Omega_c$. The growth rate remains negative for $\Omega_c < \Omega < \min[\Omega_1(d)]$ for any $d \neq 0$. Therefore, we conclude that the streamwise vortex flow is stable between $\Omega = 8.94$ and $\Omega = 9.96$ in the case of $R = 200$.

We expect a three-dimensional solution to bifurcate at Ω_1 and Ω_2. The wavenumber β in the spanwise direction of the three-dimensional solution is unchanged from that of the streamwise vortex flow because the perturbation with $b = 0$ is responsible for the bifurcation, whereas the new wavenumber α in the streamwise direction is expected to take the same value as d. Figure 3 shows two tertiary solution branches corresponding to $\alpha = 1.0$ and 0.5 with $\beta = 3.117$. The bifurcations of the tertiary solution occur at $\Omega_1 = 14.4$ and $\Omega_2 = 32.4$ for $\alpha = 1.0$ and $\beta = 3.117$, and at $\Omega_1 = 11.1$ and $\Omega_2 = 38.0$ for $\alpha = 0.5$ and $\beta = 3.117$. The bifurcations are supercritical both at Ω_1 and Ω_2 and the tertiary solutions are unique for $\Omega_1 < \Omega < \Omega_2$, i.e. the solution branches have no fold.

The stability calculations for the tertiary solutions show that the maximum real part of the growth rate $\sigma(d, b)$ takes place on $b = 0$. As the three-dimensional tertiary solution approaches its bifurcation point $\Omega = \Omega_1$, all the amplitudes of its components except $m = 0$ become smaller. Therefore, the eigenvalue $\sigma(d, 0)$ of the tertiary solution agrees with the eigenvalue $\tilde{\sigma}(m\alpha \pm d, 0)$ of the streamwise vortex flow for $m = 0, 1, 2, \cdots$, at $\Omega = \Omega_1$ as shown in figure 4. (The eigenvalues near $\Omega = \Omega_2$ behave in a similar way although they are not shown in the figure.) Figure 4 shows

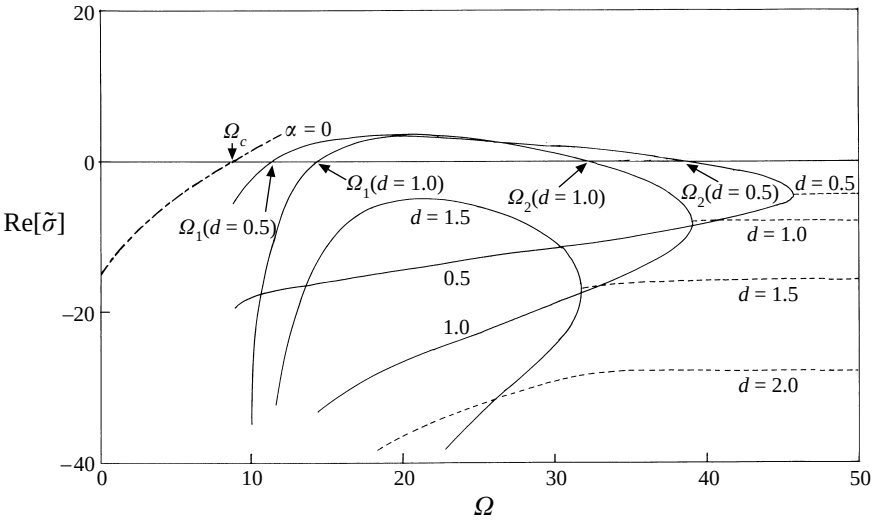

FIGURE 2. The stability of the streamwise vortex flow with $\alpha = 0$ and $\beta = 3.117$ at $R = 200$. The largest growth rate $\tilde{\sigma}$ is shown as a function of Ω for $d = 0.5, 1.0, 1.5, 2.0$ with $b = 0$. $\tilde{\sigma}$ is real on solid curves and complex on dashed curves. The dash-dotted curve represents the eigenvalue (real) of the perturbation with $d = 0, b = 3.117$ on the basic flow ($\alpha = \beta = 0$).

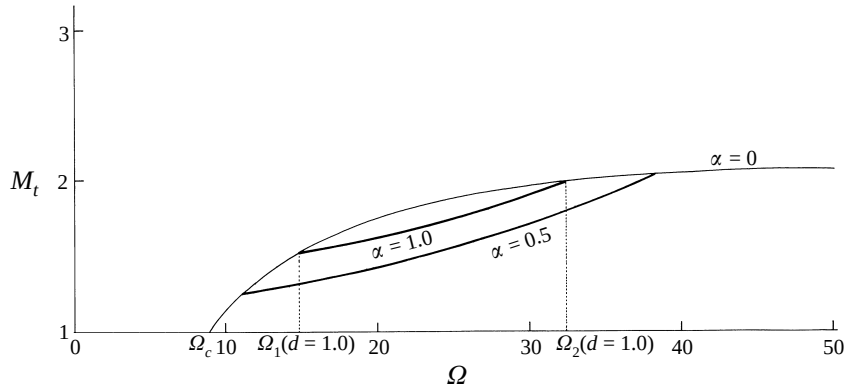

FIGURE 3. The momentum transport M_t for the nonlinear steady three-dimensional solutions with $\alpha = 1.0$, 0.5 and $\beta = 3.117$ (thick curves) at $R = 200$. The thin curve represents the nonlinear streamwise vortex flow ($\alpha = 0, \beta = 3.117$).

that the three-dimensional solution with $\alpha = 1.0$ and $\beta = 3.117$ is unstable at its bifurcation at Ω_1 and gains stability in the interval $19 < \Omega < 26.5$ to perturbations with $d = 0.5$. Further calculations have indicated that the stability range for the three-dimensional solutions is indeed determined by perturbations with $d = 0.5$. We call this instability caused by the perturbations with $d = \frac{1}{2}\alpha$ subharmonic instability.

Typical eigenvalues $\sigma(d, b)$ for the tertiary solution within the stable range are plotted on figure 5. We see that the maximum growth rate at $\Omega = 22$ takes place on $b = 0$ for fixed d. It decreases from zero at the origin as d is increased on $b = 0$. As Ω approaches the stability limit $\Omega = 19$ or 26.5, $\sigma(0.5, 0)$ increases and touches zero first.

In order to visualize the stable tertiary flow at $\Omega = 22$ we project its velocity field

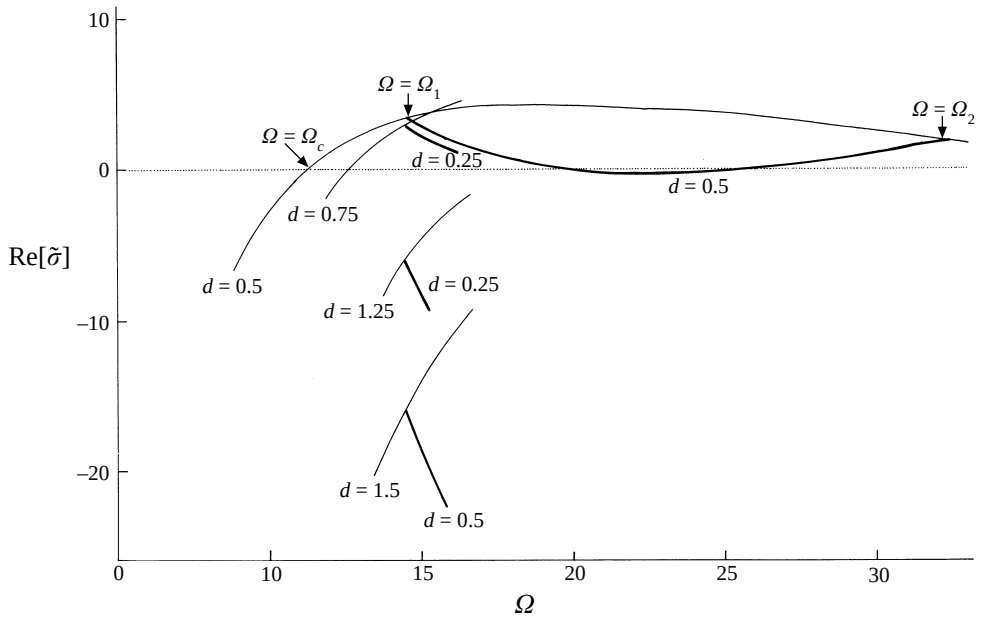

FIGURE 4. The growth rate $\tilde{\sigma}$ of the perturbation with $d = 0.5$ and 0.25 with $b = 0$ superimposed on the three-dimensional solution with $\alpha = 1.0$ and $\beta = 3.117$ (thick curves) at $R = 200$. The growth rates $\tilde{\sigma}$ of the perturbations on the streamwise vortex flows with $\alpha = 0$ and $\beta = 3.117$ are shown by thin curves for various values of d with $b = 0$.

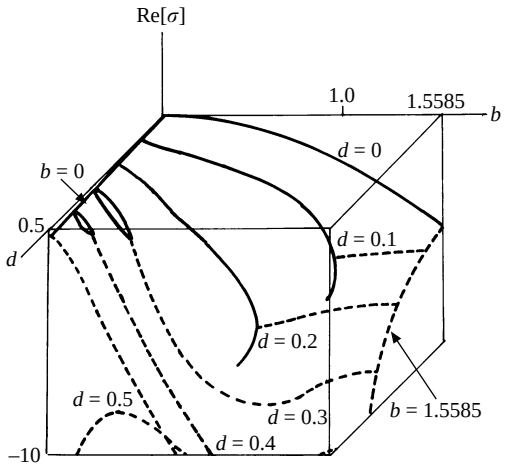

FIGURE 5. The stability of the three-dimensional solution with $\alpha = 1.0$ and $\beta = 3.117$ at $R = 200$ and $\Omega = 22$. The growth rate $\tilde{\sigma}$ is negative for any combination of d, b. The solid curves indicate real eigenvalues whereas dashed curves indicate complex eigenvalues.

at $z = 0$ onto the (x, y)-plane in figure 6. Strong streamwise currents with sinusoidal undulation in the spanwise direction characterize the flow. The streamwise currents with about a quarter of the wall speed alternate their direction on the midplane. Recall that the mean flow $\hat{U}$ vanishes on $z = 0$.

As mentioned above, $\Omega = \Omega_1(\alpha)$ is a monotonically increasing function of d. Therefore, the tertiary solution with a small α would be the first tertiary flows that

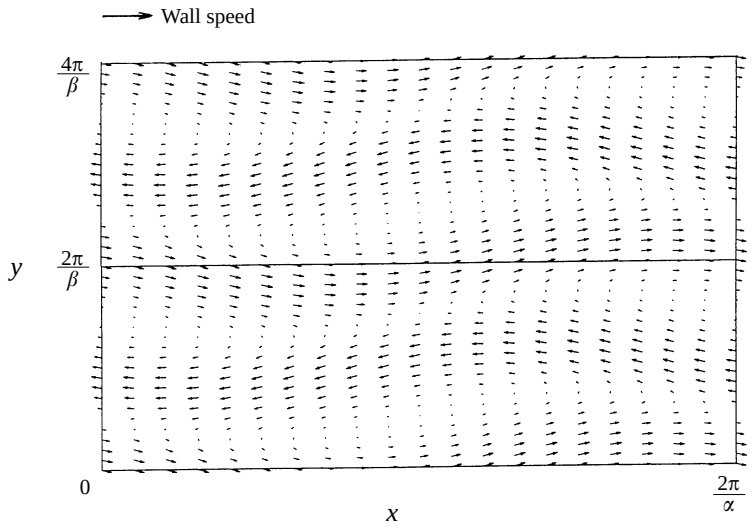

FIGURE 6. The tertiary flow with $\alpha = 1.0$ and $\beta = 3.117$ at $R = 200$ and $\Omega = 22$. The velocity field on $z = 0$ is projected on the (x, y)-plane. For reference, the magnitude of the wall speed is indicated by the arrow.

could be realized physically as Ω is increased above Ω_c. Recall that the realization of the tertiary flows would be possible only when the tertiary solution becomes stable to subharmonic mode. (The argument of the eigenvalue behaviour for the tertiary solution with $\alpha = 1.0$ in figure 4 applies to any tertiary solutions because $\Omega_1(\alpha)$ is a monotonically increasing function of d. For a fixed α the tertiary solution is unstable to the subharmonic perturbation at $\Omega = \Omega_1$.) The growth rate of the subharmonic perturbation decreases as Ω is increased and the solution gains stability at some $\Omega = \Omega_{sub}(\alpha)$. This stability boundary, $\Omega = \Omega_{sub}(\alpha)$, is indicated by a thick curve inside the curve $\Omega = \Omega_1(\alpha)$ in figure 7. The boundary, $\Omega = \Omega_{sub}(\alpha)$, is also inside $\Omega = \Omega_2(\alpha)$ since $\Omega_2(\alpha)$ is a monotonically decreasing function of d in the larger Ω region. (We were unable to extend the curve $\Omega = \Omega_{sub}(\alpha)$ for $\alpha < 0.4$ since attempts to obtain tertiary solutions for smaller α failed. The inability to obtain tertiary solutions for small α will be explained in the next subsection.) Also shown in figure 7 by a thin dashed curve is the contour of $\mathrm{Re}[\sigma] = -2$ for perturbations with $d = 0$ and $b = 0$. The imaginary part of this eigenvalue is not zero. This oscillatory mode does not reach $\mathrm{Re}[\sigma] = 0$ for $R = 200$ at least for $d > 0.4$. We shall see in the next subsection that as R is increased, the growth rate of the oscillatory mode becomes larger so that the stability region of the tertiary solution will be bounded by the oscillatory instability from inside in the (α, Ω)-plane.

5.2 $R = 400$

The stability of the secondary flow at $R = 400$ is examined in figure 8. The linear critical value $\Omega_c^{(1)}$ is 4.32 for $\alpha = 0$ and $\beta = 3.117$. The figure shows the growth rate $\tilde{\sigma}$ of perturbations with $b = 0$ for various values of d. As in the case for $R = 200$ tertiary solutions with the wavenumber $\alpha = d$ bifurcate at $\Omega = \Omega_1(d)$ and $\Omega = \Omega_2(d)$. The minimum value of $\Omega_1(d)$, $\min[\Omega(d)] = 4.71$, is determined by $d \to 0$ as in the case of $R = 200$. Recall that the maximum streamwise wavenumber that tertiary solutions can take for $R = 200$ is about $\alpha = 1.27$ (see figure 7). Figure 8 shows that the tertiary solution with $\alpha = 1.5$ is possible, indicating that the maxmum α increases for larger

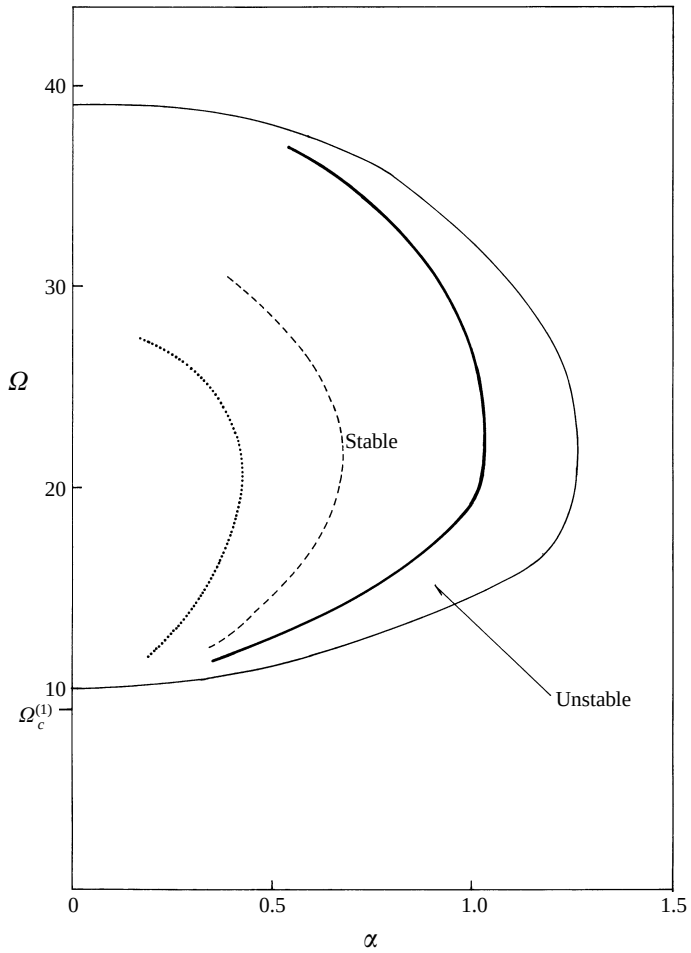

FIGURE 7. The stability of the tertiary flow. The tertiary flow is unstable at its bifurcation at $\Omega = \Omega_1(\alpha)$ (thin curve) to subharmonic perturbations and gains stability inside $\Omega = \Omega_{sub}(\alpha)$ (thick curve). The oscillatory mode with $\mathrm{Re}[\sigma] = -2$ is indicated by a dashed curve. Attempts to obtain tertiary solutions inside the dotted curve failed. $R = 200$, $\beta = 3.117$.

R. Although $d = 1.0$ has the largest growth rate in the figure, it does not mean that the tertiary solution with $\alpha = 1.0$ is most preferred.

The momentum transport M_t of three tertial solution branches for $\alpha = 0.5$, 1.0 and 1.5 with $\beta = 3.117$ is plotted in figure 9. It can be seen that the bifurcation of the tertiary solution at $\Omega = \Omega_1$ is supercritical for $\alpha = 0.5$ and subcritical for $\alpha = 1.5$. For $\alpha = 1.0$ the bifurcation occurs at $\Omega_1 = 6.498$ subcritically (but only slightly with the turning point at $\Omega \simeq 6.4955$). The bifurcated solution branch for $\alpha = 1.0$ terminates at the upper bifurcation point ($\Omega = \Omega_2 = 47.4$) supercritically, although it is not shown in the figure. For $\alpha = 0.5$ the bifurcated solution branch undergoes a sharp turning point at $\Omega \simeq 12.5$ and extends towards the small-Ω region, until it finally terminates on the solution branch for $\alpha = 1.5$ with all its harmonics, except those with the wavenumber in the x-direction that is a multiple of three of α, which vanish. (Note that the symmetry in $\mathscr{A}_2$ is unchanged by replacing α by $(3\alpha/3)$ and regarding $(\alpha/3)$ as a new wavenumber: $3m''$ and $3m'$ are still even and odd, respectively.) This

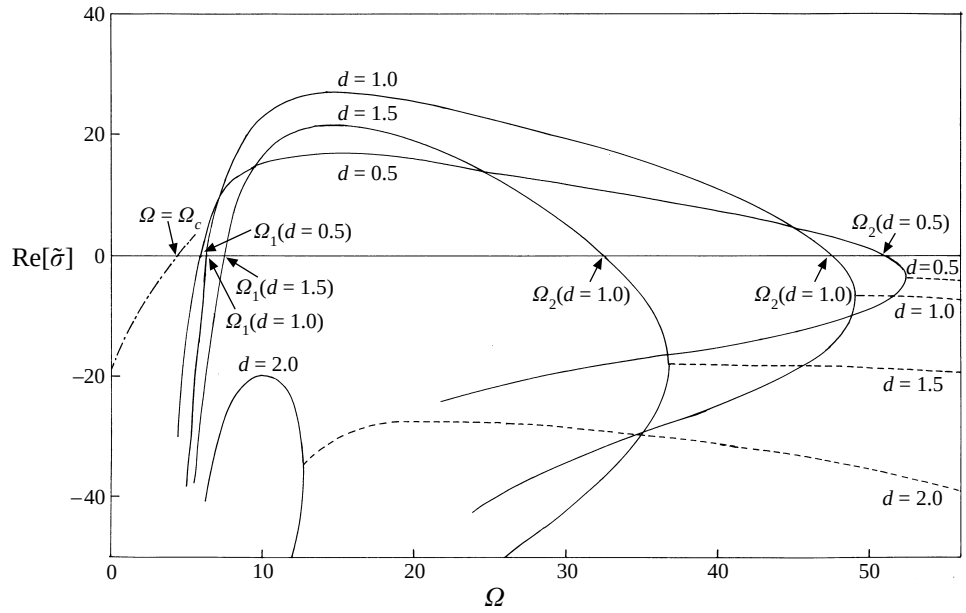

FIGURE 8. The stability of the streamwise vortex flow with $\alpha = 0$ and $\beta = 3.117$ at $R = 400$. The largest growth rate $\tilde{\sigma}$ is shown as a function of Ω for $d = 0.5, 1.0, 1.5, 2.0$ with $b = 0$. $\tilde{\sigma}$ is real on solid curves and complex on dashed curves. The dash-dotted curve represents the eigenvalue (real) of the perturbation with $d = 0, b = 3.117$ on the basic flow ($\alpha = \beta = 0$).

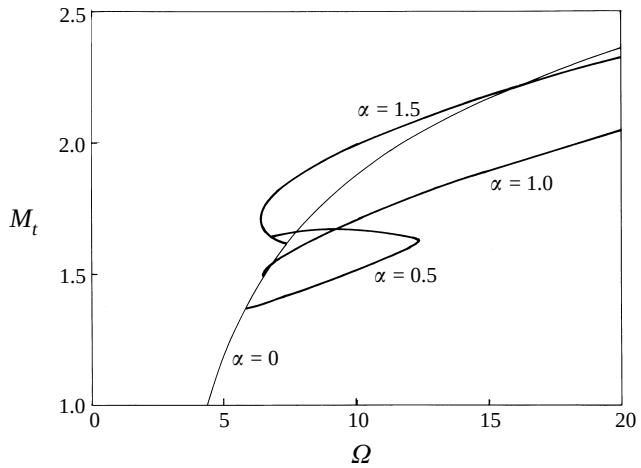

FIGURE 9. The momentum transport M_t for the nonlinear steady three-dimensional solutions (thick curves) with $\alpha = 0.5$, 1.0 and 1.5 at $R = 400$. $\beta = 3.117$. The thin curve represents the streamwise vortex flow ($\alpha = 0, \beta = 3.117$).

1 : 3 wavenumber ratio interaction is the reason for the inability to obtain tertiary solutions for small α.

The stability analysis for the bifurcated tertiary solutions shows that the solutions are unstable to subharmonic perturbations with $d = \frac{1}{2}\alpha$ and $b = 0$ at their bifurcation at $\Omega = \Omega_1$ as in the case of $R = 200$. The growth rate σ for this subharmonic mode decreases when Ω is increased for supercritical solutions ($\alpha < 1.0$). As α approaches

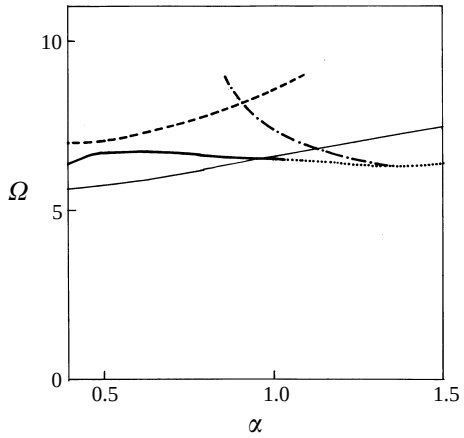

FIGURE 10. The stability of of the tertiary flow at $R = 400$. $\beta = 3.117$. The stability region is bounded by subharmonic instability $\Omega = \Omega_{sub}(\alpha)$ (thick curve) and oscillatory instabilities ($(d, b) = (0, 0)$, thick dashed curve; and $(d, b) = (\frac{1}{2}\alpha, 0)$ thick dash-dotted curve). The tertiary flow is unstable at its bifurcation at $\Omega = \Omega_1(\alpha)$ (thin curve) to subharmonic perturbations. The limit point of the subcritical solution branches is represented by a dotted curve for $\alpha > 1.0$.

1.0, the growth rate changes sharply and the subharmonic instability sets in on the lower branch of the subcritical solution for ($\alpha > 1.0$). Therefore, the curve $\Omega = \Omega_{sub}(\alpha)$ intersects with $\Omega = \Omega_1(\alpha)$ as is shown in figure 10. The intersection occurs at about $\alpha = 1.05$. Furthermore, the stability region of the tertiary solutions is bounded by oscillatory instability ($d = b = 0$) at a large Ω and by another type of oscillatory instability ($d = \frac{1}{2}\alpha, b = 0$) at a large α. The former oscillatory instability can be anticipated from the analysis for $R = 200$ (see figure 7); it has the same spatial structure as the tertiary flows, whereas the latter oscillatory instability is subharmonic in the streamwise direction. The tertiary solution at the turning point becomes unstable to this subharmonic oscillatory instability for $\alpha > 1.35$. Detailed calculations have indicated that the tertiary solution with $\alpha = 1.0$ and $\beta = 3.117$ is stable for $6.515 \leqslant \Omega \leqslant 7.4$ on the upper solution branch.

The stability of the tertiary solutions near $\Omega = \Omega_2$ is examined for $\alpha = 1.0$ and $\beta = 3.117$. At its bifurcation at $\Omega_2 = 47.4$ the tertiary solution is unstable to subharmonic modes with $d = \frac{1}{2}\alpha$ and $b = 0$. As Ω is decreased, the tertiary solution gains stability at $\Omega \simeq 42$. To demonstrate the stability at larger Ω the growth rate of perturbation at $\Omega = 35$ is plotted in the (d, b) Floquet parameter space in figure 11. At the origin $(d, b) = (0, 0)$, the eigenvalue $\sigma = 0$ always exists due to the translational invariance of the problem. The zero eigenvalue is the largest at the origin for $\Omega = 35$. As Ω is decreased from 35, the second largest eigenvalue at the origin crosses $\mathrm{Re}[\sigma] = 0$ at $\Omega \simeq 32$. This eigenvalue has non-zero imaginary part. The corresponding eigenmode is the same mode that appeared near Ω_1 as an oscillatory instability. Since the eigenvalues of the perturbations responsible for instability both at $\Omega = 6.515$ and at $\Omega = 42$ are real as in the case of $R = 200$, it appears as though the stable interval on Ω for the three-dimensional solution branch, which existed as a single interval for $R = 200$, is now divided into two parts, $6.515 \leqslant \Omega \leqslant 7.4$ and $32 \leqslant \Omega \leqslant 42$, by the appearance of a growing oscillatory mode for $R = 400$.

Both the real and the imaginary parts of σ of the oscillatory instabilities at $d = 0$ and $b = 0$ are plotted for various values of R for the tertiary solution with $\alpha = 1.0$ and $\beta = 3.117$ in figure 12. The oscillatory instability begins to emerge when $R \simeq 250$.

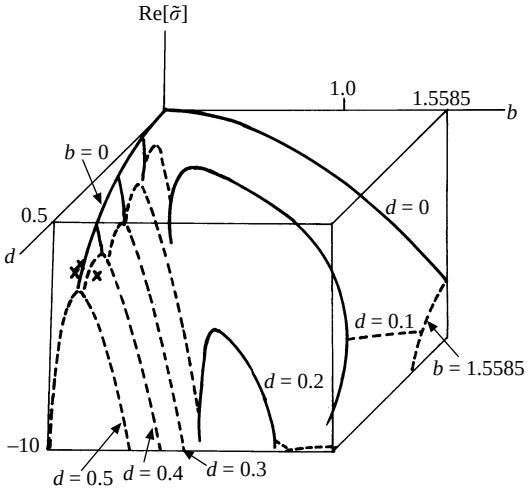

FIGURE 11. The stability of the three-dimensional solution with $\alpha = 1.0$ and $\beta = 3.117$ at $R = 400$ and $\Omega = 35$. The growth rate $\tilde{\sigma}$ is negative for any combination of d, b. The solid curves indicate real eigenvalues whereas dashed curves indicate complex eigenvalues. The three crosses show calculations at a higher truncation level $N_T = 13$ on $d = 0.5$ for $b \neq 0$ for comparison.

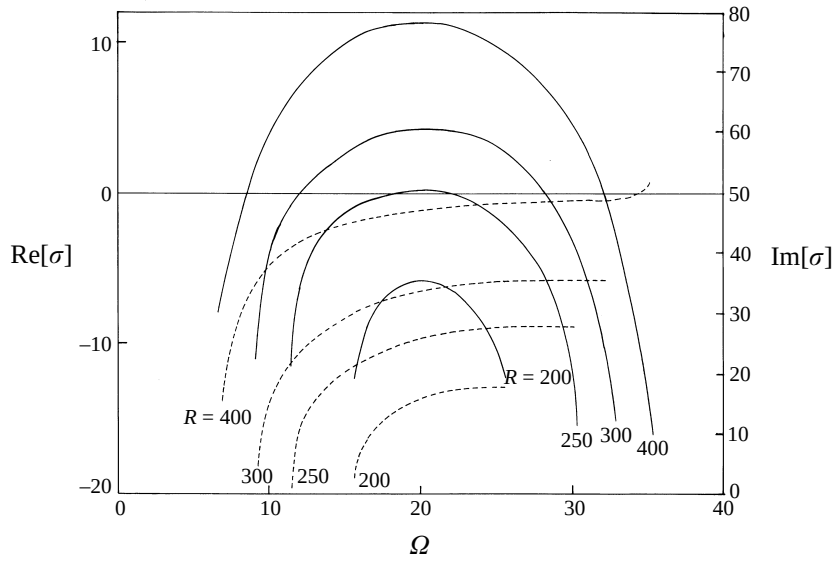

FIGURE 12. The growth rate σ of oscillatory modes with $d = b = 0$ for the three-dimensional solutions with $\alpha = 1.0$ and $\beta = 3.117$ for various values of R. The real part of σ is indicated by a solid curve, whereas the imaginary part is indicated by a dashed curve.

As R is increased, the instability spreads in the directions of both increasing and decreasing Ω. The largest growth rate always occurs around $\Omega = 20$. The imaginary part of the eigenvalue changes sharply for small Ω and levels off as Ω is increased.

Comparison of the stable tertiary motions at $\Omega = 7$ and $\Omega = 35$ in figure 13 shows that the sinusoidal spanwise undulation is larger for a higher rotation rate. The strength of the streamwise currents is not affected by the rotation rate: the magnitude

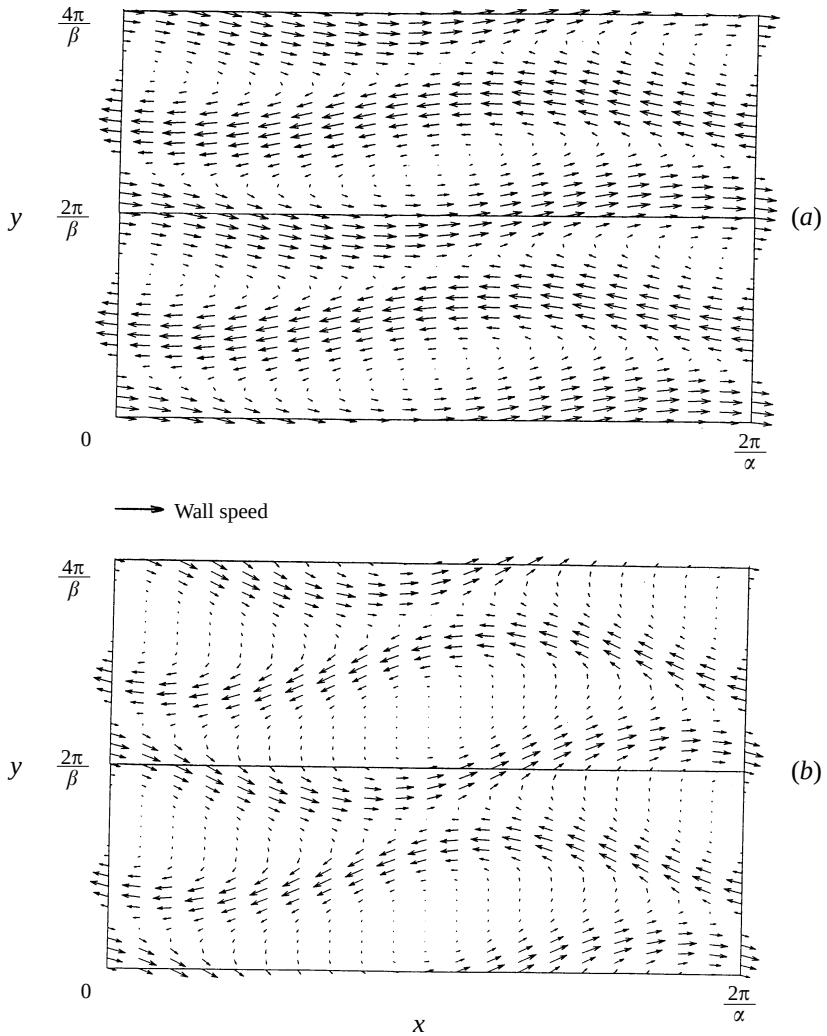

FIGURE 13. The tertiary flow with $\alpha = 1.0$ and $\beta = 3.117$ at $R = 400$. (*a*) $\Omega = 7$, and (*b*) $\Omega = 35$. The velocity field on $z = 0$ is projected on the (x, y)-plane. For reference, the magnitude of the wall speed is indicated by the arrow.

of the streamwise velocity on $z = 0$ is almost equal to a half of the wall speed for both $\Omega = 7$ and $\Omega = 35$.

5.3 $R = 600$

Without carrying out the stability anlysis of the streamwise vortex flows the steady three-dimensional solutions with $\alpha = 1.0$ and $\beta = 3.117$ for $R = 400$ are continued to $R = 600$ by gradually increasing R at a fixed Ω. The subcritical nature for $R = 600$ becomes remarkable as shown in figure 14. The subcritical region extends even in the negative-Ω region for $\alpha = 1.5$, creating two nonlinear three-dimensional solutions of plane Couette flow at $\Omega = 0$. They have already been reported by Nagata (1990). Recent analysis by Nagata (1996) using truncation levels up to $N_T = 18$ and $N'_T = 16$ shows that the minimum Reynolds number where the upper and the lower solution branches meet is $R \simeq 510$ when the wavenumbers are $\alpha = 1.15$ and $\beta = 2.35$. The

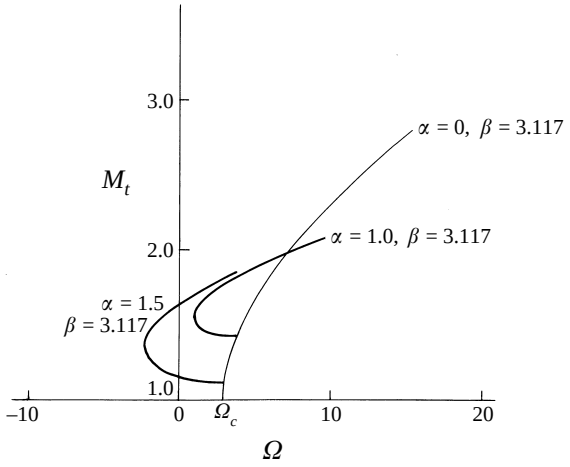

FIGURE 14. The momentum transport M_t for the nonlinear steady three-dimensional solutions at $R = 600$; $\alpha = 1.0$ and 1.5; $\beta = 3.117$.

conjecture of the abrupt bifurcation (Nagata 1990) is also supported by Conley (1994), who obtained the minimum Reynolds number of 467 at $\alpha = 0.96$ and $\beta = 2.0$ with a resolution of 11 collocation points across the fluid depth and the Fourier modes $m, n \leqslant 3$, using the Chebyshev–Tau method.

Although the accuracy of the stability analysis gets worse as R is increased, attempts to calculate the growth rate have been made for selected values of Floquet parameters d and b at $R = 600$. Preliminary results with a slightly lower truncation level ($N_T = 10$ and $N'_T = 8$) have been reported by Nagata (1993): the growth rates of subharmonic modes, $(d, b) = (\frac{1}{2}\alpha, 0)$, $(0, \frac{1}{2}\beta)$ and $(\frac{1}{2}\alpha, \frac{1}{2}\beta)$, are all positive around the fold of the three-dimensional solution branch. Therefore, it seems that the three-dimensional plane Couette flow is unstable near its abrupt bifurcation. More accurate investigation is under way.

6 Conclusion

It is found that the steady three-dimensional tertiary solutions which bifurcate from the steady streamwise vortex flows in a rotating plane Couette system are stable for relatively small Reynolds numbers within a certain range of the rotation, provided that the (constant) vorticity of the basic flow has the opposite orientation to the background rotation. The stability range in the (α, Ω)-space is bounded by subharmonic instabilities. As the Reynolds number is increased, two kinds of oscillatory instabilities set in. One of them appears in such a way that they bound the region for the stable tertiary solution from inside. The other appears at a large wavenumber α. The stable tertiary flows with wavenumbers $(\alpha, \beta) = (1.0, 3.117)$ at $R = 200$ and $R = 400$ are presented in figures 6 and 13, respectively. The flow patterns resemble the wavy motions observed by Tillmark & Alfredsson (1996) (see their figure 3*b*) at the breakdown of the stationary steamwise roll cells with spanwise width approximately equal to the gap between the two plates, i.e. $\beta \simeq \pi$, although the Reynolds number of their figure corresponds to our $R = 800$. (Their rotation number $R_o \simeq 0.01$ corresponds to our $\Omega = 8$.) The streamwise wavelength of the observed wavy pattern is approximately three times the spanwise width of the roll cells, i.e. $\beta/\alpha \simeq 3$. Although it is almost impossible to analyse the flow at $R = 800$ theoretically at present due to

the lack of accuracy, we hope that experiments will be carried out for smaller R in order to check the prediction given in the current study.

Our analysis shows that as the Reynolds number gets larger, the stability of the tertiary flows is destroyed by oscillatory instabilities. Note that there are two Hopf bifurcation points on the steady tertiary solution branch for $R > 250$ (see figure 12). A loop of a three-dimensional *time-dependent* solution connecting these two Hopf bifurcation points should be created. It may be interesting to follow the time-dependent solution branch at higher Reynolds number. As in the case of steady three-dimensional solutions, the branch may reach $\Omega = 0$, creating nonlinear time-dependent solutions in a plane Couette system. This time-dependent flow could be a standing wave solution, completely different from those shape-preserving three-dimensional travelling wave solutions recently obtained by Nagata (1997), where the bifurcation of plane Couette flow mixed with a plane Poiseuille flow was considered.

It should be noted that the non-rotating plane Couette flow is rather special among shear motions in the sense that the spanwise vorticity is destributed homogeneously across the fluid layer. This homegeneous distribution of the spanwise vorticity of the basic flow seems to be related to the absence of the instability due to the Orr–Sommerfeld mode. The absence of linear instabilities had hampered nonlinear analyses in plane Couette flow until the discovery of the nonlinear steady three-dimensional solution by Nagata (1990). Recently, three-dimensional plane Couette flow solutions were detected by Clever & Busse (1992) in the limit of vanishing Rayleigh number in Bénard convection with a plane Couette system. They are identical to the solution by Nagata (1990). More recently, Cherhabili & Ehrenstein (1997) reported spatially localized structures both in the two-dimensional case (unstable) and in the three-dimensional case (stability not analysed) by continuing nonlinear travelling wave solutions in plane Poiseuille flow to the plane Couette flow limit. It is likely that all the steady equilibrium states obtained in plane Couette flow so far are unstable and physically unrealizable. The sinusoidal flow patterns presented in this paper and in Nagata (1990) resemble the spatially organized structure observed during a quasi-cyclic regeneration process of the turbulent structure of plane Couette flow examined by direct numerical simulations (Hamilton, Kim & Waleffe 1995). Resemblance is so good that we believe the equilibrium state found by Nagata (1990) plays an important role as an unstable fixed point in subcritical transition of the Navier–Stokes system (Waleffe 1995).

The absence of tertiary solutions for small α must be investigated in detail in conjunction with the mode interaction with the wavenumber ratio 1 : 3. As in the Rayleigh–Bénard convection new solutions may arise (Nagata 1995).

Appendix

The set $\mathscr{A}_2$ for the steady three-dimensional solutions is represented by

$$\phi : \left\{ \begin{array}{l} \cos m'\alpha x \cos n'\beta y\, f_{\ell'}(z) \\ \cos m''\alpha x \cos n''\beta y\, f_{\ell''}(z) \\ \cos m'\alpha x \sin n''\beta y\, f_{\ell''}(z) \\ \cos m''\alpha x \sin n'\beta y\, f_{\ell'}(z) \\ \sin m'\alpha x \cos n'\beta y\, f_{\ell''}(z) \\ \sin m''\alpha x \cos n''\beta y\, f_{\ell'}(z) \\ \sin m'\alpha x \sin n''\beta y\, f_{\ell'}(z) \\ \sin m''\alpha x \sin n'\beta y\, f_{\ell''}(z) \end{array} \right\}, \quad \psi : \left\{ \begin{array}{l} \cos m'\alpha x \cos n''\beta y\, \sin \ell''\pi(z+\tfrac{1}{2}) \\ \cos m''\alpha x \cos n'\beta y\, \sin \ell'\pi(z+\tfrac{1}{2}) \\ \cos m'\alpha x \sin n'\beta y\, \sin \ell'\pi(z+\tfrac{1}{2}) \\ \cos m''\alpha x \sin n''\beta y\, \sin \ell''\pi(z+\tfrac{1}{2}) \\ \sin m'\alpha x \cos n''\beta y\, \sin \ell'\pi(z+\tfrac{1}{2}) \\ \sin m''\alpha x \cos n'\beta y\, \sin \ell''\pi(z+\tfrac{1}{2}) \\ \sin m'\alpha x \sin n'\beta y\, \sin \ell''\pi(z+\tfrac{1}{2}) \\ \sin m''\alpha x \sin n''\beta y\, \sin \ell'\pi(z+\tfrac{1}{2}) \end{array} \right\}, \quad \text{(A 1)}$$

where m', n', and ℓ' stand for odd integers, whereas m'', n'', and ℓ'' stand for even integers.

The two-dimensional streamwise vortex flows, $\mathscr{U}_0$ in Nagata (1986), can be recovered from the above expression by disregarding all the contributions except $m'' = 0$:

$$\phi : \left\{ \begin{array}{l} \cos n''\beta y\, f_{\ell''}(z) \\ \sin n'\beta y\, f_{\ell'}(z) \end{array} \right\}, \quad \psi : \left\{ \begin{array}{l} \cos n'\beta y\, \sin \ell'\pi(z+\tfrac{1}{2}) \\ \sin n''\beta y\, \sin \ell''\pi(z+\tfrac{1}{2}) \end{array} \right\}. \tag{A 2}$$

The restriction of (A 1) to spanwise-independent flows, on the other hand, could be achieved by keeping only those contributions with $n'' = 0$:

$$\phi : \left\{ \begin{array}{l} \cos m''\alpha x\, f_{\ell''}(z) \\ \sin m''\alpha x\, f_{\ell'}(z) \end{array} \right\}, \quad \psi : \left\{ \begin{array}{l} \cos m'\alpha x\, \sin \ell''\pi(z+\tfrac{1}{2}) \\ \sin m'\alpha x\, \sin \ell'\pi(z+\tfrac{1}{2}) \end{array} \right\}. \tag{A 3}$$

Although the Orr–Sommerfeld mode (two-dimensional flow with $\partial_y \equiv 0$ and $\psi \equiv 0$) is included in (A 3) (regard 2α as the primary wavenumber for ϕ), the non-zero contribution of ψ in this restriction suggests that the set $\mathscr{A}_2$ does not originate directly from the instability due to the Orr–Sommerfeld mode. The three-dimensional representation $\mathscr{A}_1$ whose restriction to $n'' = 0$ is identical to the Orr–Sommerfeld mode is listed in Nagata (1986).

Four classes for perturbations imposed on the steady three-dimensional solution $\mathscr{A}_2$ are described below.

Class A: $d = 0,\ b \neq 0$

$$\tilde{\phi}, \tilde{\psi} : \left\{ \begin{array}{l} \cos m''\alpha x \cos n''\beta y\, F_{\ell''}(z) \\ \cos m''\alpha x \sin n''\beta y\, F_{\ell''}(z) \\ \cos m''\alpha x \cos n'\beta y\, F_{\ell'}(z) \\ \cos m''\alpha x \sin n'\beta y\, F_{\ell'}(z) \\ \sin m'\alpha x \cos n''\beta y\, F_{\ell''}(z) \\ \sin m'\alpha x \sin n''\beta y\, F_{\ell''}(z) \\ \sin m'\alpha x \cos n'\beta y\, F_{\ell'}(z) \\ \sin m'\alpha x \sin n'\beta y\, F_{\ell'}(z) \\ \cos m'\alpha x \cos n''\beta y\, F_{\ell'}(z) \\ \cos m'\alpha x \sin n''\beta y\, F_{\ell'}(z) \\ \cos m'\alpha x \cos n'\beta y\, F_{\ell''}(z) \\ \cos m'\alpha x \sin n'\beta y\, F_{\ell''}(z) \\ \sin m''\alpha x \cos n''\beta y\, F_{\ell'}(z) \\ \sin m''\alpha x \sin n''\beta y\, F_{\ell'}(z) \\ \sin m''\alpha x \cos n'\beta y\, F_{\ell''}(z) \\ \sin m''\alpha x \sin n'\beta y\, F_{\ell''}(z) \end{array} \right\}, \tag{A 4}$$

Class B: $d = 0,\ b \neq 0$

$$\tilde{\phi}, \tilde{\psi} : \left\{ \begin{array}{l} \cos m' \alpha x \cos n'' \beta y \, F_{\ell''}(z) \\ \cos m' \alpha x \sin n'' \beta y \, F_{\ell''}(z) \\ \cos m' \alpha x \cos n' \beta y \, F_{\ell'}(z) \\ \cos m' \alpha x \sin n' \beta y \, F_{\ell'}(z) \\ \sin m'' \alpha x \cos n'' \beta y \, F_{\ell''}(z) \\ \sin m'' \alpha x \sin n'' \beta y \, F_{\ell''}(z) \\ \sin m'' \alpha x \cos n' \beta y \, F_{\ell'}(z) \\ \sin m'' \alpha x \sin n' \beta y \, F_{\ell'}(z) \\ \cos m'' \alpha x \cos n'' \beta y \, F_{\ell'}(z) \\ \cos m'' \alpha x \sin n'' \beta y \, F_{\ell'}(z) \\ \cos m'' \alpha x \cos n' \beta y \, F_{\ell''}(z) \\ \cos m'' \alpha x \sin n' \beta y \, F_{\ell''}(z) \\ \sin m' \alpha x \cos n'' \beta y \, F_{\ell'}(z) \\ \sin m' \alpha x \sin n'' \beta y \, F_{\ell'}(z) \\ \sin m' \alpha x \cos n' \beta y \, F_{\ell''}(z) \\ \sin m' \alpha x \sin n' \beta y \, F_{\ell''}(z) \end{array} \right\}, \tag{A 5}$$

Class C: $d \neq 0,\ b = 0$

$$\tilde{\phi} : \left\{ \begin{array}{l} \cos m'' \alpha x \cos n'' \beta y \, F_{\ell''}(z) \\ \cos m'' \alpha x \cos n'' \beta y \, F_{\ell'}(z) \\ \cos m'' \alpha x \cos n' \beta y \, F_{\ell''}(z) \\ \cos m'' \alpha x \cos n' \beta y \, F_{\ell'}(z) \\ \sin m'' \alpha x \cos n'' \beta y \, F_{\ell''}(z) \\ \sin m'' \alpha x \cos n'' \beta y \, F_{\ell'}(z) \\ \sin m'' \alpha x \cos n' \beta y \, F_{\ell''}(z) \\ \sin m'' \alpha x \cos n' \beta y \, F_{\ell'}(z) \\ \cos m' \alpha x \sin n'' \beta y \, F_{\ell''}(z) \\ \cos m' \alpha x \sin n'' \beta y \, F_{\ell'}(z) \\ \cos m' \alpha x \sin n' \beta y \, F_{\ell''}(z) \\ \cos m' \alpha x \sin n' \beta y \, F_{\ell'}(z) \\ \sin m' \alpha x \sin n'' \beta y \, F_{\ell''}(z) \\ \sin m' \alpha x \sin n'' \beta y \, F_{\ell'}(z) \\ \sin m' \alpha x \sin n' \beta y \, F_{\ell''}(z) \\ \sin m' \alpha x \sin n' \beta y \, F_{\ell'}(z) \end{array} \right\}, \qquad \tilde{\psi} : \left\{ \begin{array}{l} \cos m' \alpha x \cos n'' \beta y \, F_{\ell''}(z) \\ \cos m' \alpha x \cos n'' \beta y \, F_{\ell'}(z) \\ \cos m' \alpha x \cos n' \beta y \, F_{\ell''}(z) \\ \cos m' \alpha x \cos n' \beta y \, F_{\ell'}(z) \\ \sin m' \alpha x \cos n'' \beta y \, F_{\ell''}(z) \\ \sin m' \alpha x \cos n'' \beta y \, F_{\ell'}(z) \\ \sin m' \alpha x \cos n' \beta y \, F_{\ell''}(z) \\ \sin m' \alpha x \cos n' \beta y \, F_{\ell'}(z) \\ \cos m'' \alpha x \sin n'' \beta y \, F_{\ell''}(z) \\ \cos m'' \alpha x \sin n'' \beta y \, F_{\ell'}(z) \\ \cos m'' \alpha x \sin n' \beta y \, F_{\ell''}(z) \\ \cos m'' \alpha x \sin n' \beta y \, F_{\ell'}(z) \\ \sin m'' \alpha x \sin n'' \beta y \, F_{\ell''}(z) \\ \sin m'' \alpha x \sin n'' \beta y \, F_{\ell'}(z) \\ \sin m'' \alpha x \sin n' \beta y \, F_{\ell''}(z) \\ \sin m'' \alpha x \sin n' \beta y \, F_{\ell'}(z) \end{array} \right\}, \tag{A 6}$$

Class D: $d \neq 0,\ b = 0$

$$\tilde{\phi}: \left\{ \begin{array}{l} \cos m''\alpha x \sin n''\beta y\, F_{\ell''}(z) \\ \cos m''\alpha x \sin n''\beta y\, F_{\ell'}(z) \\ \cos m''\alpha x \sin n'\beta y\, F_{\ell''}(z) \\ \cos m''\alpha x \sin n'\beta y\, F_{\ell'}(z) \\ \sin m''\alpha x \sin n''\beta y\, F_{\ell''}(z) \\ \sin m''\alpha x \sin n''\beta y\, F_{\ell'}(z) \\ \sin m''\alpha x \sin n'\beta y\, F_{\ell''}(z) \\ \sin m''\alpha x \sin n'\beta y\, F_{\ell'}(z) \\ \cos m'\alpha x \cos n''\beta y\, F_{\ell''}(z) \\ \cos m'\alpha x \cos n''\beta y\, F_{\ell'}(z) \\ \cos m'\alpha x \cos n'\beta y\, F_{\ell''}(z) \\ \cos m'\alpha x \cos n'\beta y\, F_{\ell'}(z) \\ \sin m'\alpha x \cos n''\beta y\, F_{\ell''}(z) \\ \sin m'\alpha x \cos n''\beta y\, F_{\ell'}(z) \\ \sin m'\alpha x \cos n'\beta y\, F_{\ell''}(z) \\ \sin m'\alpha x \cos n'\beta y\, F_{\ell'}(z) \end{array} \right\}, \qquad \tilde{\psi}: \left\{ \begin{array}{l} \cos m'\alpha x \sin n''\beta y\, F_{\ell''}(z) \\ \cos m'\alpha x \sin n''\beta y\, F_{\ell'}(z) \\ \cos m'\alpha x \sin n'\beta y\, F_{\ell''}(z) \\ \cos m'\alpha x \sin n'\beta y\, F_{\ell'}(z) \\ \sin m'\alpha x \sin n''\beta y\, F_{\ell''}(z) \\ \sin m'\alpha x \sin n''\beta y\, F_{\ell'}(z) \\ \sin m'\alpha x \sin n'\beta y\, F_{\ell''}(z) \\ \sin m'\alpha x \sin n'\beta y\, F_{\ell'}(z) \\ \cos m''\alpha x \cos n''\beta y\, F_{\ell''}(z) \\ \cos m''\alpha x \cos n''\beta y\, F_{\ell'}(z) \\ \cos m''\alpha x \cos n'\beta y\, F_{\ell''}(z) \\ \cos m''\alpha x \cos n'\beta y\, F_{\ell'}(z) \\ \sin m''\alpha x \cos n''\beta y\, F_{\ell''}(z) \\ \sin m''\alpha x \cos n''\beta y\, F_{\ell'}(z) \\ \sin m''\alpha x \cos n'\beta y\, F_{\ell''}(z) \\ \sin m''\alpha x \cos n'\beta y\, F_{\ell'}(z) \end{array} \right\}. \quad \text{(A 7)}$$

Here, for simplicity, $F_{\ell'}(z)$ and $F_{\ell''}(z)$ represent $f_{\ell'}(z)$ and $f_{\ell''}(z)$ for $\tilde{\phi}$, or $\sin \ell' \pi(z+\frac{1}{2})$ and $\sin \ell'' \pi(z+\frac{1}{2})$ for $\tilde{\psi}$. It should be added that when dealing with the stability of streamwise vortex flows, only those components with $m'' = 0$ are retained in classes C and D: they are classified as $\tilde{\mathscr{U}}_I$ and $\tilde{\mathscr{U}}_{II}$ in Nagata (1986).

REFERENCES

Alfredsson, P. H. & Persson, H. 1989 Instabilities in channel flows with system rotation. *J. Fluid Mech.* **202**, 543.

Andereck, C. D., Dickman, R. & Swinney, H. L. 1983 New flows in a circular Couette system with co-rotating cylinders. *Phys. Fluids* **26**, 1395.

Bradshaw, P. 1969 The analogy between streamline curvature and buoyancy in turbulent shear flow. *J. Fluid Mech.* **36**, 177.

Bradshaw, P. 1988 Near-wall turbulence. *Zoran Zaric Memorial Conference* (ed. S. J. Kline & N. H. Afghan). Hemisphere.

Chandrasekhar, S. 1961 *Hydrodynamic and Hydromagnetic Stability*. Oxford University Press.

Cherhabili, A. & Ehrenstein, U. 1997 Finite-amplitude equilibrium states in plane Couette flow. *J. Fluid Mech.* **342**, 159.

Clever, R. M. & Busse, F. H. 1992 Three dimensional convection in a horizontal fluid layer subject to a constant shear. *J. Fluid Mech.* **234**, 511.

Conley, A. 1994 New plane shear flows. PhD thesis, California Institute of Technology.

Finlay, W. H. 1989 Perturbation expansion and weakly nonlinear analysis for two-dimensional vortices in curved or rotating channels. *Phys. Fluids* A **1**, 854.

Finlay, W. H. 1990 Transition to oscillatory motion in rotating channel flow. *J. Fluid Mech.* **215**, 209.

Hamilton, J. M., Kim, J. & Waleffe, F. 1995 Regeneration mechanisms of near-wall turbulence structures. *J. Fluid Mech.* **287**, 317.

Hart, J. F. 1971 Instability and secondary motion in a rotating channel flow. *J. Fluid Mech.* **45**, 341.

Hopfinger, E. J. 1989 Turbulence and vortices in rotating fluids. In *Theoretical and Applied Mechanics* (ed. P. Germain, M. Piau & D. Caillerie), p. 177. Elsevier.

Hopfinger, E. J. & Linden P. F. 1990 The effect of background rotation on fluid motions: a report on Euromech 245. *J. Fluid Mech.* **211**, 417.

Lezius, D. K. & Johnston, J. P. 1976 The structure and stability of turbulent boundary layers in rotating channel flow. *J. Fluid Mech.* **77**, 153.

Nagata, M. 1986 Bifurcations in Couette flow between almost corotating cylinders. *J. Fluid Mech.* **169**, 229.

Nagata, M. 1988 On wavy instabilities of the Taylor-vortex flow between corotating cylinders. *J. Fluid Mech.* **188**, 585.

Nagata, M. 1990 Three-dimensional finite amplitude solutions in plane Couette flow. *J. Fluid Mech.* **217**, 519.

Nagata, M. 1993 Stability of non-axisymmetric flows in the Taylor-Couette system. In *Unstable and Turbulent Motion of Fluid* (ed. S. Kida), p. 3. World Scientific.

Nagata, M. 1995 Bifurcations at the Eckhaus points in two-dimensional Rayleigh-Bénard convection. *Phys. Rev.* E **52**, 6141.

Nagata, M. 1996 Nonlinear solutions of the modified plane Couette flow in the presence of a transverse magnetic field. *J. Fluid Mech.* **307**, 231.

Nagata, M. 1997 Three-dimensional traveling-wave solution in plane Couette flow. *Phys. Rev.* E **55**, 2023.

Tillmark, N. & Alfredsson, P. H. 1996 Experiments on rotating plane Couette flow. In *Advances in Turbulence VI* (ed. S. Gavrilakis, L. Machiels & P. A. Monkewitz), p. 391. Kluwer.

Tritton, D. J. 1978 Turbulence in rotating fluids. In *Rotating Fluids in Geophysics* (ed. P. H. Roberts & A. M. Soward), p. 105. Academic.

Tritton, D. J. 1985 Experiments on turbulence in geophysical fluid dynamics. In *Turbulence and Predictability in Geophysical Fluid Dynamics and Climate Dynamics* (ed. M. Ghil), p. 172. North-Holland.

Tritton, D. J. & Davies, P. A. 1981 Instabilities in geophysical fluid dynamics. In *Hydrodynamic Instabilities and the Transition to Turbulence*. Topics in Applied Physics (ed. H. L. Swinney & J. P. Gollub), vol. 45, p. 229. Springer.

Waleffe, F. 1995 Transition in shear flows. Nonlinear normality versus non-normal linearity. *Phys. Fluids* **7**, 3060.

Yang, K.-S. & Kim, J. 1991 Numerical investigation of instability and transition in rotating plane Poiseuille flow. *Phys. Fluids* A **3**, 633.